RANS Simulations of a GCH4/GOx Single Element Combustor

By A. Chemnitz, M. Schulze AND T. Sattelmayer

Institute of Thermodynamics, Technische Universität München
Boltzmannstr. 15, 85747 Garching b. München

The reacting flow inside a coaxial single element combustor for gaseous methane and oxygen is simulated, using the commercial tool Fluent. The simulation is conducted in a context of thermoacoustic stability analysis and aims at producing appropriate mean fields rather than highly resolved flow features. Therefore the focus is set on methods of comparatively low computational effort. The first approach, carried out during the SFB/TRR 40 Summer Program, is documented in this report. The steady state RANS equations are solved using the k-ω-SST-Model in combination with a steady diffusion flamelet approach. To reduce the computational effort, the originally rectangular combustion chamber is approximated by an axis-symmetric two-dimensional geometry. The numerical results are evaluated regarding internal flow fields and compared to experimental data. These were obtained at the Institute for Flight Propulsion at TUM. The test case provides experimental results for the wall chamber pressure as well as data for wall temperature and heat flux. The latter are derived quantities from temperature measurements inside the chamber structure. The numerical results are found to capture the global tendency of the validation data, however further work is necessary to satisfactory predict local developments and quantitative values.

1. Introduction

The thermoacoustic instability in rocket combustion chambers is a topic of high relevance for the design process of a rocket engine. Although instabilities in the combustion process have shown to be a major issue for a long time [1], their sufficient prediction is still a matter of ongoing research. At the Institute of Thermodynamics the corresponding work focuses on cost effective approaches with a potential for industrial application. Thereto a hybrid approach is taken [2, 3]. This basically results in the decomposition of the case under consideration into three parts:

- Calculation of the mean flow field
- Determination of the Flame Transfer Function
- Linearized analysis of acoustic perturbations

The mean flow field describes the unperturbed flow, i.e. the state before the onset of a potential instability. Potential driver for combustion instabilities is the response of the flame to flow perturbations. This response is modeled via a Flame Transfer Function (FTF). It can be derived from excited transient simulations [4]. Providing the mean flow field and the FTF, the development of acoustics perturbations is studied using the Linearized Euler Equations (LEE). This is done either in time space or via a frequency space approach.

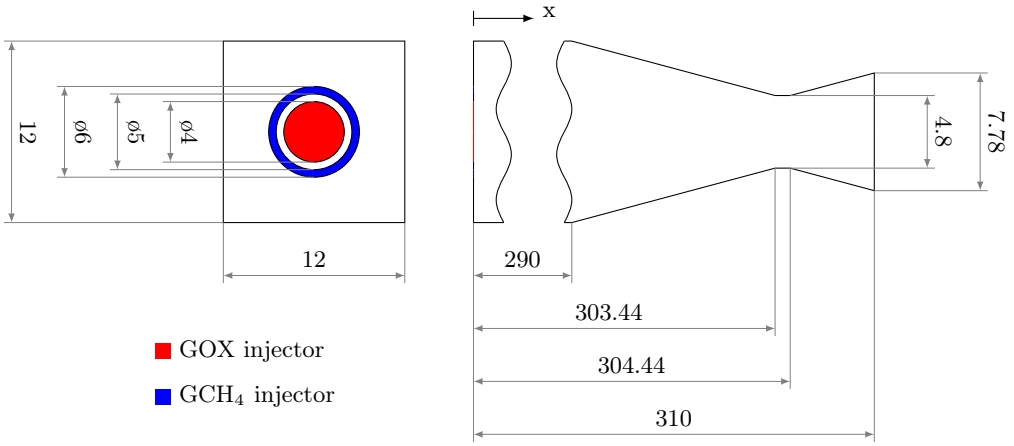

FIGURE 1. Main chamber dimensions; in mm

The method described above has been used with hydrogen/oxygen systems. For further studies the procedure shall be applied to methane rocket combustion chambers as well. Thereto capabilities have to be established in all three steps. In the beginning the mean flow field inside a methane combustion chamber is to be calculated. This requires capturing the effects of mixing and combustion. The prediction of both processes is necessary for the subsequent determination of the FTF as well. Since the goal is to provide a mean flow sufficient for performing stability analysis rather than capturing single flow details, in a first approach low effort methods are employed. In the first place this refers to the solution of the Reynolds-averaged Navier-Stokes equations (RANS). To capture the complex chemistry of methane combustion, while avoiding expensive kinetic calculations, a flamelet model is chosen. It has to be noted that the work presented here is just a preliminary approach to this type of set up and will be continued to improve the quality of the numerical predictions.

This work has been carried out in the frame of the SFB/TRR 40 Summer Program. There an operating point of the single element methane combustor of the Institute for Flight Propulsion (LFA) has been studied numerically. The results are validated against wall pressure and heat flux profiles provided in the test case definition [5]. In addition the internal flow fields, mainly the species distributions, are presented.

2. Reference Experiment

The setup under consideration is a single element combustion chamber of the LFA. A detailed description of the experiment can be found in [5]. In the following a short description of the combustor and the operating conditions will be given.

The combustion chamber has a rectangular crossection with an edge length of 12 mm and an overall length of 310 mm. The nozzle is two-dimensional with an contraction ratio of 2.5. At the faceplate the propellants are injected coaxial with oxygen at the center. The main dimensions of the chamber are summarized in Fig. 1.

The chamber is equipped with thermocouples in the vertical and horizontal symmetry plane as well as pressure transducers to capture the pressure distribution along the chamber wall. The temperature profile at the chamber wall is calculated from the mea-

surements and provided as boundary condition in the test case definition. It is plotted in Fig. 2 in section 3. For comparison of experimental and numerical data, the wall pressure profile as well as the reconstructed wall heat flux are available (cf. section 4). In addition mass flows and temperatures of the propellants upstream of the injector are given which will be used as boundary conditions (cf. section 3).

The combustor is capacitively cooled leading to a transient temperature distribution at the chamber wall. The data provided for boundary conditions and validation are averaged over an interval of 0.5 s.

3. Numerical Setup

In this section the main numeric aspects of the presented work are discussed. This refers to the modeling of basic flow features, species properties as well as computational grids used and boundary conditions.

3.1. *General Approach*

For the calculation of the flow field the RANS equations for steady flow are solved. This is done using the pressure based coupled solver of the commercial tool Fluent. For turbulence closure the two equations k-ω-SST-Model [6] is applied. Turbulent species and enthalpy transport are included via turbulent Schmidt and Prandtl numbers, both set to a value of 0.85. The near wall behavior of turbulence is accounted for by Low-Re-Corrections [7]. The reaction inside the chamber is modeled using a steady laminar diffusion flamelet approach. Thereby turbulence influences are included via a β-PDF. Local species compositions are then obtained by interpolation over mixture fraction, its variance and scalar dissipation. The model can be considered as semi-diabatic with the influence of the local enthalpy being included for the temperature but not for the species composition.

3.2. *Boundary Conditions and Species Modeling*

The relevant boundary conditions are summarized in Tab. 1. The procedure for setting boundary conditions for kinetic energy and specific dissipation rate from the specified turbulence intensity I and turbulence length scale l_t is given in [7]. The faceplate is treated as adiabatic no-slip wall. For the chamber wall the temperature profile from the measurements is used as thermal boundary condition. Due to the two-dimensionality, only one boundary is required. The corresponding values are taken from the profiled side of the chamber. They are given in [5] and shown in Fig. 2.

The species thermodynamic data are determined from NASA-Polynomials [8]. In the case under consideration heat transfer and thus thermal conductivity in the wall near regions are of importance. Accordingly special attention has to be paid to the modeling of this quantity. The transport properties are calculated via the approach described in [8] with the thermal conductivity taken as its frozen part. The mixture transport properties are determined from the temperature dependent species values, thereby taking interaction between different species into account.

For the generation of the flamelets a sub-mechanism of a reaction mechanism from the DLR has been used, comprising 21 species and 97 reactions.

3.3. *Mesh*

To reduce computational effort with regard to the very basic approach of this work, the three dimensional chamber is approximated using a two dimensional grid. The rectan-

Boundary	Type	Specification		
		Mass flux	Turbulence	Temperature
Injector O_2	Mass flow	3581 $\frac{kg}{m^2 s}$	I = 0.05; l_t=0.07 D_h	278 K
Injector CH_4	Mass flow	1968 $\frac{kg}{m^2 s}$	I = 0.05; l_t=0.07 D_h	269 K
Chamber wall	no-slip wall	-	Resolved BL	Profile

TABLE 1. Relevant boundary conditions; D_h: hydraulic diameter

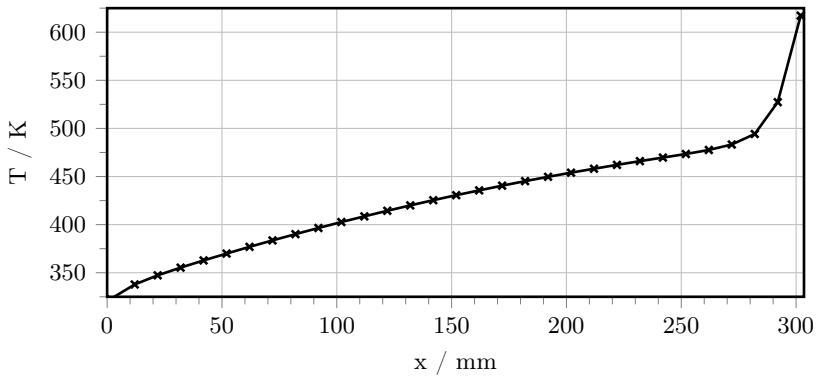

FIGURE 2. Temperature boundary condition along the chamber wall

$r_{chamber}$	r_{throat}	r_{exit}
mm	mm	mm
6.77	4.28	5.68

TABLE 2. Radii of simplified chamber geometry

gular cross section is replaced by a circular shape with the areas of chamber, nozzle throat and nozzle exit held constant. The resulting dimensions are given in Tab. 2. The mesh is based on a common reference grid designed by several groups attending the summer program. So far three successively refined grids have been used to study the influence of grid spacing. The size of the wall adjacent cell is kept constant during refinement. For all grids the condition $y^+ < 1$ is satisfied at the wall. Basic parameters for the different meshes are listed in Tab. 3.

4. Results

In this section the numerical results are evaluated. First the grid influence is assessed, followed by a validation against experimental data. It has to be kept in mind that data obtained with a rectangular chamber are compared to computations carried out for an axis-symmetric geometry. Finally internal flow fields are considered and the overall results are discussed. Since experimental data are only available in the combustion chamber, the focus is set on this region rather than the nozzle section.

Mesh	No. of cells (radial / axial)	Radial spacing mm	Axial spacing mm	Injector spacing mm	Wall resolution mm
1	46e3 (121 / 377)	2e-4 - 0.17	0.10 - 1.00	0.10	2e-4 - 5e-4
2	91e3 (168 / 541)	2e-4 - 0.12	0.07 - 0.71	0.07	2e-4 - 5e-4
3	175e3 (225 / 776)	2e-4 - 0.09	0.05 - 0.50	0.05	2e-4 - 5e-4

TABLE 3. Basic mesh parameters

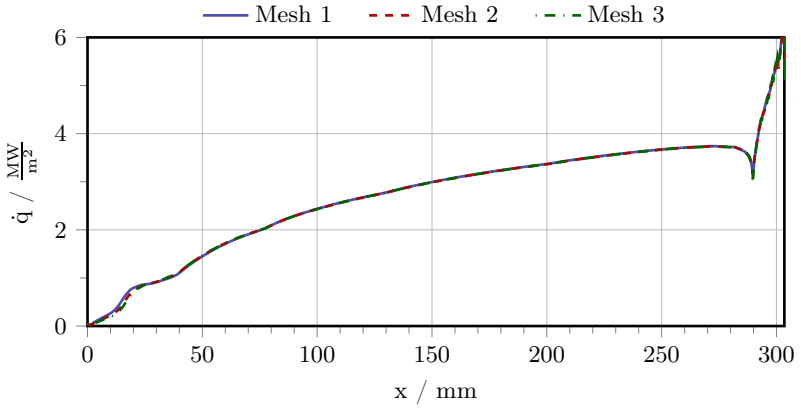

FIGURE 3. Wall heat flux for different meshes

4.1. *Grid Influence*

For the visualization of grid influence the computed heat flux distribution for the three meshes is shown in Fig. 3. While the rear part of the chamber does not show any significant influence of the grid on the heat flux, this is not the case in the area close to the faceplate. There a slight increase of the heat flux can be seen when the mesh is refined. However, compared to the whole chamber, this area is small and thus should not exhibit a strong influence on global parameters. This is confirmed by the pressure distribution (not shown) which does not show any significant influence of the grid. At the current status of this ongoing work global trends are more important than the exact resolution of local flow phenomena. Thus the obtained level of grid convergence is acceptable for the moment without more detailed studies.

4.2. *Comparison to Experimental Data*

For an assessment of the quality of the computations, experimentally determined parameters are extracted from the results and compared to their measured values. Available data are the wall pressure distribution as well as the wall heat flux.

The wall pressure distribution is shown for experiment and simulation in Fig. 4. The absolute pressure values show a difference of about 2 to 3 bar along the whole length of the chamber. The qualitative development is studied via the normalized pressure profiles (p_{norm}). They are obtained by dividing the pressure by its value at the last measurement position (x = 272.5 mm). The relative pressure difference along the chamber length is captured fairly well as can be seen from the coincidence of the numerical and experimental normalized pressure at the faceplate. The numeric as well as the experimental

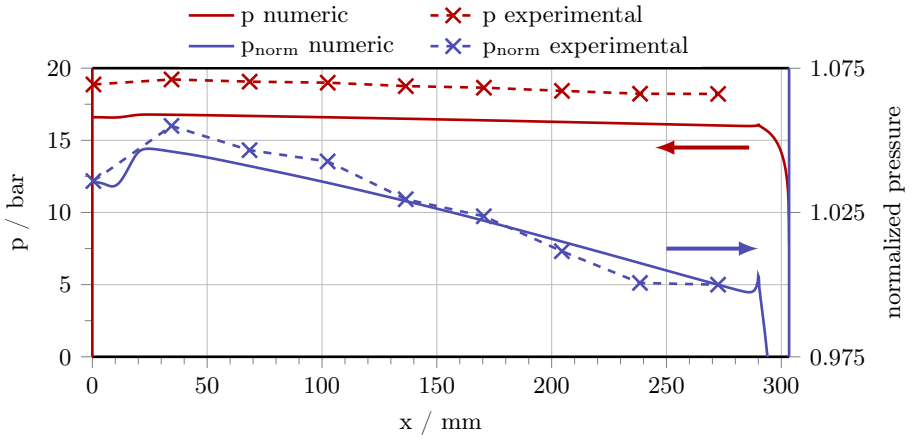

FIGURE 4. Absolute and normalized pressure distribution

profile reach their respective maximum value in the front part of the chamber and decrease further downstream. However, the axial development of the normalized profiles shows different tendencies between the initial and the last measurement point. After reaching its maximum value, the numerically determined distribution decreases continuously, showing a smooth shape without a change of curvature (i.e. left/right curved). In contrast the experimental results posses a far more complex structure. However, the number of measurement positions does not allow specific conclusions regarding curvature or kinks of the curve. Downstream of x = 240 mm the experimental pressure distribution appears to form a plateau, while no such tendency is present in the computational results.

The computed wall heat flux is shown in Fig. 5 along with its validation data from the experiment. Apparently the current prediction underestimates the wall heat flux by about 20 to 30%. The strongest deviation occurs near the faceplate. As with the pressure distribution the computational curve is much smoother than the validation data. These show a local peak at x $\approx$ 20 mm with a slight decrease downstream. From x $\approx$ 35 mm on the wall heat flux increases again. Those tendencies are visible in the numeric curve as well; however they remain less pronounced. That is there are analog changes in curvature and gradient respectively, while no local extremum occurs. Further downstream the numeric curve again stays smooth and without a change of curvature, whereas the validation data show a more complex development.

4.3. *Internal Flow Field*

Beyond the prediction of parameters to be compared with the experiment, the numerical simulation gives access to the internal flow. The temperature field is shown in Fig. 6 together with the mixture fraction. The region of highest temperatures does not reach the chamber axis but keeps a considerable distance throughout the whole chamber. This indicates a long flame with poor mixing. Further affirmation comes from the mixture fraction which shows a strong stratification, persisting until the chamber exit.

In the test case definition information regarding the distribution of main species are requested to allow for better comparison of different results. The spatial distribution of species mass fractions across the chamber are given in Fig. 7(a) to 7(c). The weak mixing mentioned above reflects in the species distribution as well. While the stratification is

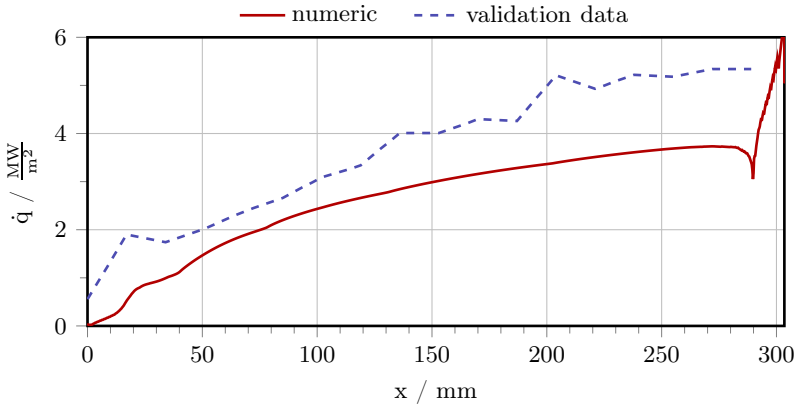

FIGURE 5. Wall heat flux

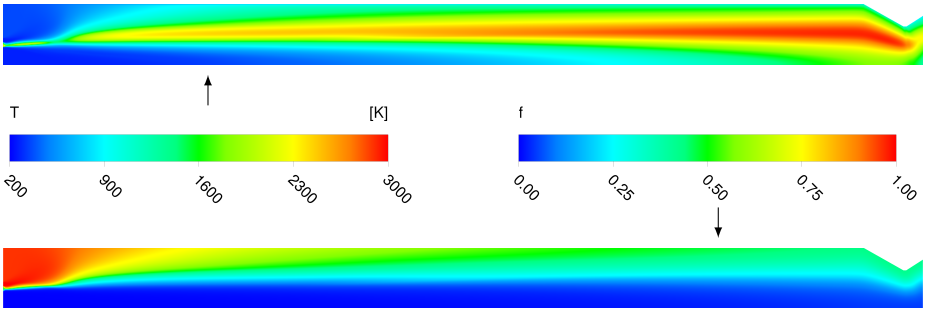

FIGURE 6. Temperature T and mixture fraction f

visible especially in the educts (Fig. 7(a)), the intermediates and final products (Fig. 7(b) and 7(c)) show highest mass fractions in the middle and outer part of the chamber with a weak reacting core around the chamber axis.

The axial evolution of the species mass fractions is shown in Fig. 8. The values were computed by radial mass flow averaging and are plotted along with their equilibrium values, obtained using the CEA-code [8]. Considering the educts, especially O_2 shows a significant difference to its equilibrium value at the chamber exit. There the CFD simulation predicts much more unburned oxidizer than the equilibrium calculation. Regarding products and intermediate species, CO_2 nearly reaches its equilibrium value, while H_2O, CO and OH stay significantly below theirs. Figure 8(c) shows the OH mass fraction along the chamber axis. Across the whole chamber it lies below the corresponding averaged value. This again visualizes the radial stratification inside the chamber.

4.4. *Discussion*

Compared with the experimental and validation data, both wall heat flux and chamber pressure are underestimated by the simulation. The chamber pressure depends on heat release and heat loss through the wall, the first increasing and the last decreasing it. The fact that, although the wall heat flux is underestimated, the chamber pressure lies below its experimental values indicates a notable lack in the current heat release prediction. The mixture fraction and species distribution show a strong stratification of the flow suggesting poor mixing as the main reason for the low heat release. The comparison

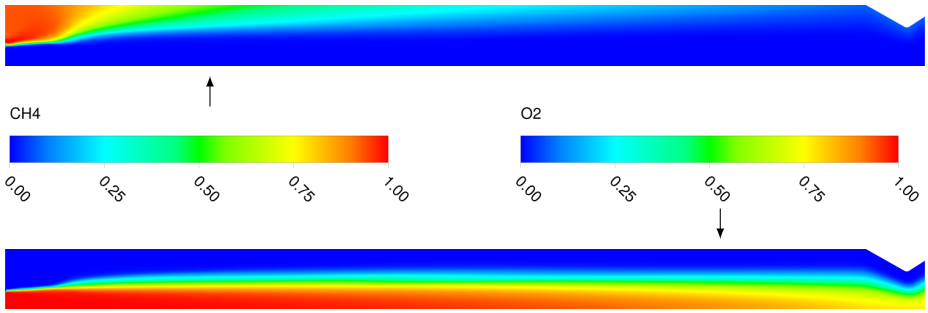

(a) Mass fractions of CH_4 and O_2

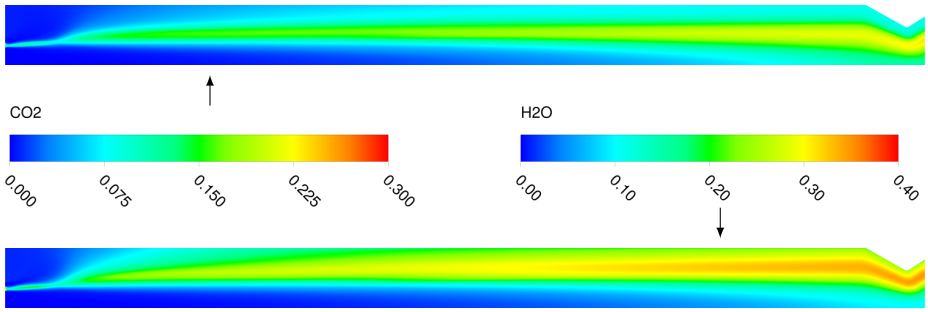

(b) Mass fractions of CO_2 and H_2O

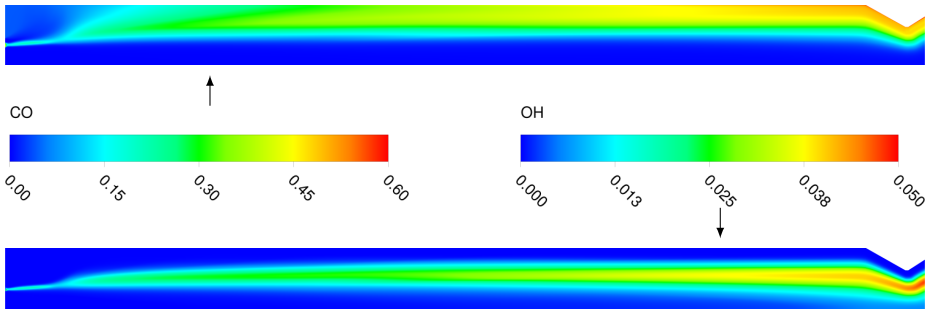

(c) Mass fractions of CO and OH

FIGURE 7. Internal flow field

of the axial species distribution with its equilibrium values indicates an uncompleted reaction at the chamber exit as well. There notable residuals of unburned oxygen remain and product mass fractions lie below their equilibrium values.

5. Conclusion

The reacting flow inside a single element oxygen/methane rocket combustion chamber has been computed numerically. Thereto a flamelet approach combined with steady RANS equations has been applied using the k-ω-SST-model for turbulence closure. The

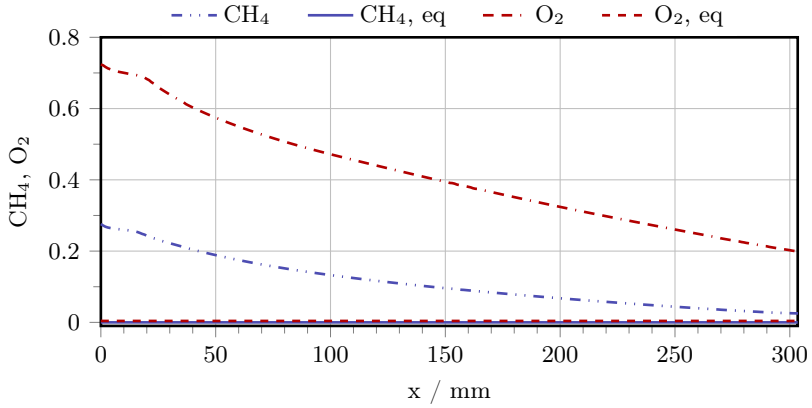

(a) CH_4 and O_2

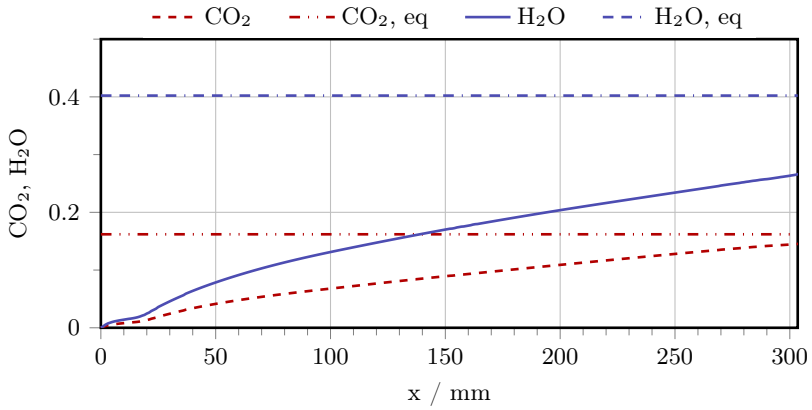

(b) CO_2 and H_2O

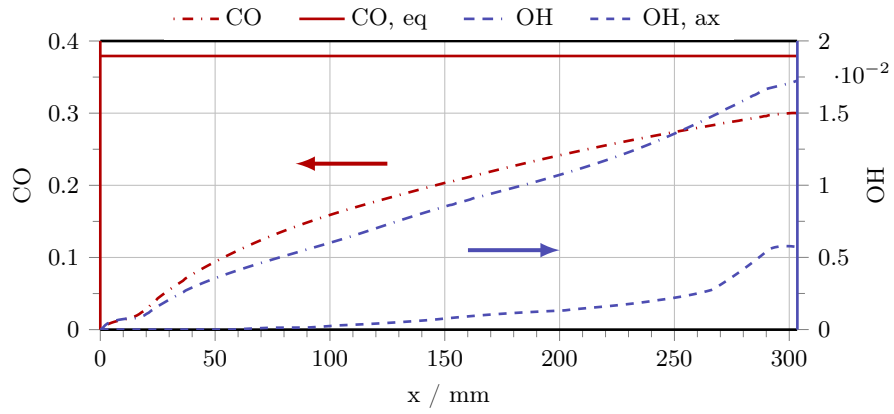

(c) CO and OH ($OH_{eq} \approx 0.03$)

FIGURE 8. Axial evolution of species mass fractions; radial mass flow average; equilibrium value (eq); value at symmetry axis (ax)

influence of the computational grid on the results has been studied and found acceptable for the current state of work.

A comparison to experimental data has shown that, while the global tendencies are captured, the local as well as the quantitative predictions of the flow fields are not satisfactory yet. Namely the wall heat flux and chamber pressure are underpredicted in the siumlation. The possible main reason is the underestimation of heat release due to poor numerical mixing in the flow. This can be seen from the combination of underestimated wall heat flux and chamber pressure together with the internal flow fields. Temperature and species distributions, directly linked to the mixture fraction, show a strong radial stratification and a departure from chemical equilibrium at the chamber exit.

The work on this topic is to be continued in order to improve agreement between predictions and simulation. This may include the adaption of modeling parameters in the RANS-equations as well as the incorporation of an increased degree of turbulence resolution like Detached Eddy Simulations (DES).

Acknowledgments

Financial support has been provided by the German Research Foundation (Deutsche Forschungsgemeinschaft – DFG) in the framework of the Sonderforschungsbereich Transregio 40.

References

[1] SUTTON, G. P. AND BIBLARZ, O. (2001). *Rocket Propulsion Elements*. John Wiley & Sons.

[2] SCHULZE, M., SCHMID, M., MORGENWECK, D., KÖGLMEIER, S. AND SATTELMAYER, T. (2012). *A Conceptional Approach for the Prediction of Thermoacoustic Stability in Rocket Engines*. Sonderforschungsbereich/Transregio 40 – Anual Report 2012.

[3] SCHULZE, M. AND SATTELMAYER, T. (2014). *Time and Frequency Domain Descriptions of Thermoacoustics in Rocket Engines with Focus on Dome Coupling - A Comparison* . Sonderforschungsbereich/Transregio 40 – Anual Report 2014.

[4] SCHULZE, M. AND SATTELMAYER, T. (to be published). *Flamedynamics in Supercritical H2/O2 Rocket Combustion Systems*. Sonderforschungsbereich/Transregio 40 – Anual Report 2015.

[5] CELANO, M. P., SIMONA, S., KIRCHBERGER, C., SCHLIEBEN, G., KNAB, O. AND HAIDN, O.. *Transregio SFB-TR40 – Test Case 1*.

[6] MENTER, F. R. (1994). *Two-Equation Eddy-Viscosity Turbulence Models for Engineering Applications*. *AIAA Journal*, **32(8)**.

[7] *Fluent Theory Guide*. Product Documentation ANSYS Inc. Release 15.0.

[8] GORDON, S. AND MCBRIDE, B. J. (1994). *Computer Program for Calculation of Complex Chemical Equilibrium Compositions and Applications – I. Analysis*. NASA Reference Publication 1311.